



Turbulent drag on a low-frequency vibrating grid in superfluid ^4He at very low temperatures

D. I. Bradley, S. N. Fisher,* A. M. Guénault, R. P. Haley, Mukesh Kumar, C. R. Lawson, Roch Schanen, P. V. E. McClintock, Lydia Munday, G. R. Pickett, Malcolm Poole, V. Tsepelin, and Paul Williams

Physics Department, Lancaster University, Lancaster, LA1 4YB, United Kingdom

(Received 11 May 2012; published 28 June 2012)

We present measurements of the dissipative turbulent drag on a vibrating grid in superfluid ^4He over a wide range of (low) frequencies. At high velocities, the dissipative drag is independent of frequency and is approximately the same as that measured in normal liquid ^4He . We present measurements on a similar grid in superfluid $^3\text{He-B}$ at low temperatures which shows an almost identical turbulent drag coefficient at low frequencies. However, the turbulent drag in $^3\text{He-B}$ is substantially higher at higher frequencies. We also present measurements of the inertial drag coefficient for grid turbulence in ^4He . The inertial drag coefficient is significantly reduced by turbulence in both superfluid and normal liquid ^4He .

DOI: [10.1103/PhysRevB.85.224533](https://doi.org/10.1103/PhysRevB.85.224533)

PACS number(s): 67.25.dg, 67.30.eh, 67.25.dk, 47.27.Cn

I. INTRODUCTION

Turbulence is ubiquitous in nature and has far-reaching technological and scientific impacts. Turbulence in classical fluids has been studied for a very long time, but is still poorly understood and difficult to predict. Superfluid ^4He and superfluid $^3\text{He-B}$ at very low temperatures are often considered as ideal fluids since, in the absence of any normal fluid component, they have zero viscosity and are (almost) incompressible. In a superfluid, vortices are quantized: they all have the same circulation given by the circulation quantum $\kappa = h/m_4$ ($h/2m_3$) for ^4He ($^3\text{He-B}$) where m_4 (m_3) is the bare mass of a helium-4 (helium-3) atom. Quantum turbulence (QT) corresponds to a tangle of such vortex lines.¹⁻³ At low temperatures, in the absence of externally imposed currents, the resultant superfluid flow is determined entirely by the vortex line configuration and so it is conceptually simpler and easier to model.⁴⁻⁶ (This is not the case at higher temperatures where there is a significant normal fluid component which can also become turbulent.) Recent experiments at low temperatures⁷⁻¹³ have shown that pure QT has a number of similarities to classical turbulence. An understanding of QT might therefore impact on understanding turbulence in general.

The simplest way to generate QT in a pure superfluid is by making it flow past a surface at a sufficiently high velocity. At low velocities, superfluids flow without any dissipation whatsoever. This is demonstrated quite spectacularly by their ability to support persistent (super)currents.^{14,15} Above some critical velocity, however, the superfluid flow becomes dissipative. According to Landau,^{16,17} excitation production, corresponding to dissipation, can occur when the velocity exceeds $v_L = (E/p)_{\min}$, where $E(p)$ is the excitation energy as a function of its momentum p . For superfluid ^4He , the minimum value of E/p for excitations occurs close to the roton minimum of the dispersion curve which gives a critical velocity of $v_L \approx \Delta_0/p_0 \approx 50 \text{ m s}^{-1}$, where Δ_0 and p_0 are the energy and momentum of rotons at the roton minimum. The Landau critical velocity in superfluid ^4He has only been observed directly in experiments on negative ions propagating in isotopically pure ^4He ;¹⁸ in other experiments, the observed critical velocities are normally very much lower.

The critical velocity for macroscopic objects moving in superfluid ^4He is typically of the order of a few cm s^{-1} and is

due to vortex growth from the remanent vortices that are almost universally present^{19,20} and are pinned to surface roughness. In the presence of superfluid flow, these vortices may interact and reconnect with themselves and with each other in a complex fashion to produce QT. Much higher critical velocities can be achieved when special care is taken to minimize the density of remanent vortices.²¹ The critical velocities and the drag force exerted at higher velocities are quite easy to measure with mechanical resonators. Oscillatory turbulent flows in superfluid ^4He were first investigated using torsional oscillators²² and U-tubes.^{23,24} Recent measurements have been made with vibrating wire resonators,^{21,25-27} tuning forks,²⁸⁻³⁰ levitating spheres,³¹ and electrostatically driven grids.^{32,33}

It is particularly interesting to study the behavior of grids. Uniform flow through grids has been used extensively to study homogenous isotropic turbulence in classical fluids.^{34,35} The study of homogenous isotropic turbulence is very important for testing the basic theoretical models of turbulence.^{1,3,36} It is difficult to generate uniform superfluid flow through a grid at very low temperatures. However, a towed grid device has been made for superfluid turbulence measurements at higher temperatures,^{37,38} and a similar device is currently being constructed for intended use at very low temperatures.³⁹ It is far easier to generate oscillatory flows at very low temperatures through the use of vibrating objects. Vibrating grids have also been used to study classical turbulence⁴⁰⁻⁴² and they have been used extensively to study QT in superfluid ^3He at ultralow temperatures.⁴³ Recently we have developed a technique for generating and detecting large-amplitude, low-frequency, grid oscillations⁴⁴ which has the potential to generate an approximation to homogenous isotropic QT at very low temperatures. Below we describe such a device and we present measurements of both the dissipative and the inertial drag forces which it experiences as it produces QT. We show that dissipative drag is independent of frequency at high velocities, thus providing a good indication that the device behaves in the same way as it would for uniform flow.

II. EXPERIMENT

The vibrating grid used in the current experiments is shown in Fig. 1. The frame of the device is formed by a 100- μm insulated copper-clad single filament NbTi wire bent into a

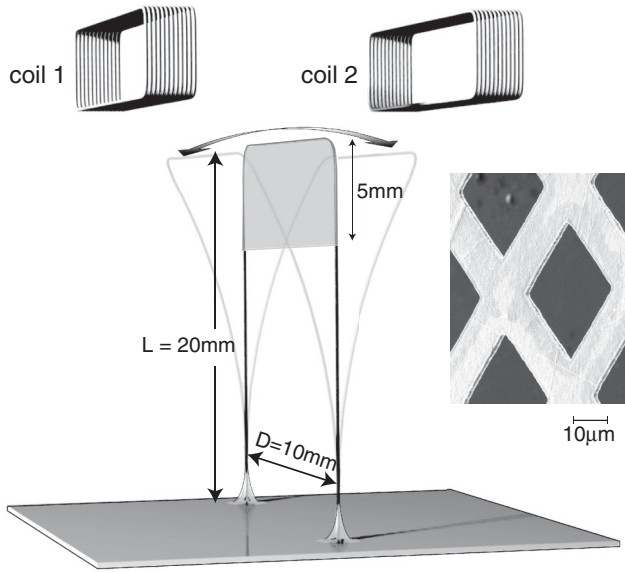


FIG. 1. Schematic of the vibrating grid device with two pickup coils used to measure its position. Inset shows an electron microscope image of the copper grid mesh.

goalpost shape as shown in the figure. The height of the goalpost is $L = 20$ mm and the length of the crossbar (the leg spacing) is $D = 10$ mm. A 5×10 mm rectangular piece of fine copper grid mesh is attached to the top of the goalpost using a very small amount of Stycast 1266. The inset to Fig. 1 shows an electron micrograph of the mesh. The mesh is approximately $1 \mu\text{m}$ thick and has $23 \mu\text{m}$ square holes separated by $11 \mu\text{m}$ copper strips, giving a repeat length of $34 \mu\text{m}$. The edges of the copper strips which form the mesh are rounded on the scale of $\sim 0.1 \mu\text{m}$ and surface roughness/irregularities are also visible on this length scale.

The device is mounted in a cylindrical epoxy cell which is installed in a Lancaster dilution refrigerator that has a base temperature below 3 mK.⁴⁵ For thermal contact, the cell contains a small $\sim 2 \times 8 \times 12$ mm silver sinter pad which is connected, via a high-purity annealed 1 mm silver wire, to a larger silver sinter pad in the mixing chamber of the refrigerator. The crossbar of the vibrating grid is located roughly 1 mm below the top end cap of the cell. Two pickup coils are fixed to the outside of the top end cap and are positioned on either side of the device as indicated in Fig. 1. The coils are made from 135 turns of $140 \mu\text{m}$ insulated copper-clad single core NbTi superconducting wire. The coils are used to detect the position of the grid as detailed in Sec. V below.

The device is operated in a vertical magnetic field of $B = 82$ mT provided by a large superconducting magnet located in the 4.2 K helium bath surrounding the refrigerator. The device has a well-defined narrow resonance in vacuum at $T = 4.2$ K with a center frequency of 59.55 Hz and a frequency width of 0.95 Hz.

III. VELOCITY MEASUREMENTS

The device can be operated in the same fashion as a vibrating wire resonator.^{25,46} It is driven by the Lorentz force which acts on its crossbar when an ac drive current $I_0 \exp(i\omega t)$

is passed through the wire frame. The amplitude of the driving force is

$$F_0 = BDI_0. \quad (1)$$

The driving current is supplied by a function generator.

As the device moves through the vertical magnetic field, a voltage V is induced across the crossbar, proportional to its velocity v ,

$$V = BDv. \quad (2)$$

The induced voltage is measured by a lock-in amplifier referenced to the function generator. The velocity amplitude v_0 of the motion is then obtained from the measured voltage amplitude V_0 using Eq. (2).

Velocity measurements of this type are usually confined to frequencies in the vicinity of the resonant frequency of the device. Far from resonance, the output is often dominated by background voltages, arising from the wire inductance and “cross talk” between the leads. The present device allows measurements at arbitrary frequencies, using the pickup coils to measure the position of the crossbar. This will be described in Sec. V. First we present our measurements of the grid response at its resonant frequency.

IV. RESONANT RESPONSE

The measured response at resonance, using the velocity measurement technique, is shown in Fig. 2. Here we plot the velocity amplitude v_0 of the crossbar of the grid, inferred from Eq. (2), as a function of the amplitude F_0 of the driving force given by Eq. (1). The measurements were made while slowly stepping up the amplitude of the driving current. The drive frequency was adjusted for each measurement to maintain the grid on resonance. We define the resonant frequency as being that at which the velocity of the grid is precisely in phase with the driving force; in practice the measurement program adjusts the frequency to maintain the out-of-phase component of the

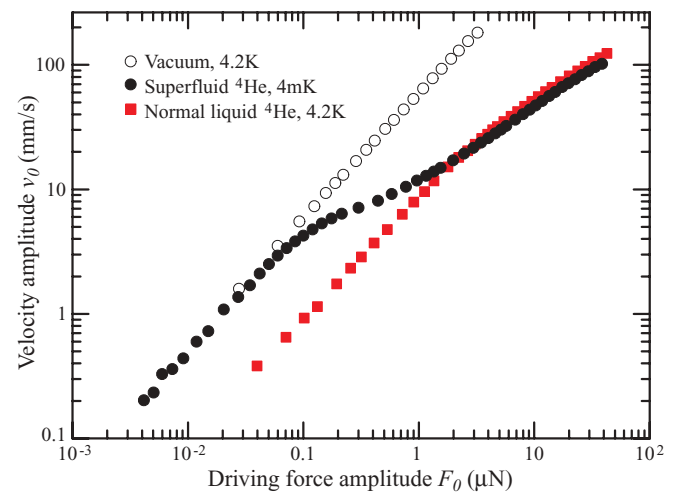


FIG. 2. (Color online) The velocity amplitude of the vibrating grid as a function of the driving force at the resonant frequency. Red squares show measurements taken in normal liquid at 4.2 K. Filled circles show measurements taken at the lowest temperatures, ~ 4 mK. Open circles show measurements taken in vacuum at 4.2 K (see text).

velocity below some specified value, typically below 1% of the in-phase velocity. At the resonant frequency the driving force amplitude is equal to the amplitude of the dissipative drag force since the inertial and restoring forces exactly balance.

Figure 2 shows the response for three different conditions: in vacuum, in normal liquid ^4He at 4.2 K, and in superfluid ^4He at very low temperatures. For the latter measurements, the temperature could not be determined precisely because there was no independent thermometer in the cell. However, we expect the temperature of the cell to be fairly close to that of the mixing chamber temperature which was measured to be ~ 4 mK. The response of vibrating objects in superfluid ^4He is typically found to become temperature independent below ~ 100 mK,³¹ so these measurements are clearly in the zero-temperature limit.

In vacuum, the response is quite linear over the entire range of velocities. In normal liquid ^4He at low velocities, the backflow is laminar and the corresponding dissipative drag force is governed by the fluid viscosity.⁴⁷ In the zero-temperature limit, the superfluid undergoes pure potential flow at low velocities and there is no viscous damping. In this case, the damping should be dominated by internal dissipation within the object itself. Indeed, the measurements in Fig. 2 show that the low velocity response of the grid at the lowest temperatures is quite close to the response measured in vacuum at 4.2 K (see below for a more detailed comparison). At higher velocities the response in the liquid becomes nonlinear, which we attribute to the generation of vortices and turbulence.

A. The turbulent drag coefficient

It is convenient to characterize the drag forces on an object by a dimensionless drag coefficient C_d defined by⁴⁸

$$F = \frac{1}{2}\rho v^2 A C_d, \quad (3)$$

where A is the cross-sectional area of the object perpendicular to the motion (for a grid, this is the solid area of the mesh) and ρ is the density of the fluid. For oscillatory flow, we take F and v in Eq. (3) to be the amplitudes of the dissipative drag force and velocity oscillations, respectively. The resulting drag coefficients, corresponding to the data in Fig. 2, are shown in Fig. 3.

At low velocities, the drag coefficient is roughly inversely proportional to the velocity amplitude of the grid, corresponding to the linear force-velocity response. At higher velocities, the drag coefficient in the normal liquid appears to be tending towards a constant value of order unity, which is typical for turbulent flows in classical fluids. At high velocities, the drag coefficient in superfluid helium is seen to be similar to that in normal helium, showing that the dissipative turbulent drag for fully developed quantum turbulence is similar to that of classical turbulence.

To obtain the fluid contribution to the drag force, we need to subtract the internal drag forces F_i :

$$F_f(v, T) = F(v, T) - F_i(v, T). \quad (4)$$

For the measurements at 4.2 K, we take $F_i(v, T)$ to be the directly measured vacuum response at 4.2 K shown in Fig. 2. It is difficult to measure the vacuum damping at lower temperatures due to thermal decoupling. In practice the vacuum responses

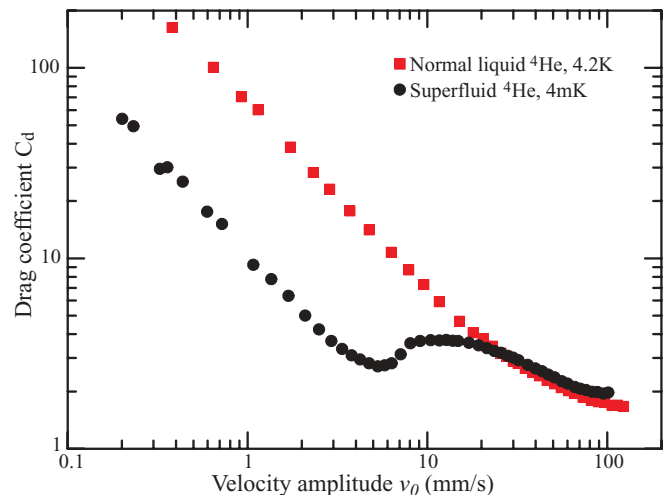


FIG. 3. (Color online) The dissipative drag coefficient of the vibrating grid, at its resonant frequency, as a function of its velocity amplitude. Red squares show measurements taken in normal liquid ^4He at 4.2 K. Black circles show measurements taken at the lowest temperatures, ~ 4 mK, see text.

of most mechanical resonators do not change drastically on cooling below 4 K, so we may use the vacuum measurements at 4.2 K as a rough approximation for the vacuum response at the lower temperatures. However, to obtain a precise value we have adjusted the measured force by a multiplicative factor of 1.19 to ensure that the fluid force vanishes at low velocities. This may indicate that the internal dissipative forces on the grid are 19% higher at the lowest temperatures. However, without having a direct measurement of the vacuum damping at the lowest temperatures, we cannot rule out the possibility that the extra damping at low velocities arises from the superfluid. There are at least two possible mechanisms for this: acoustic emission and dissipation from remanent vortices. Acoustic emission should be entirely negligible at these low oscillation frequencies,⁴⁹ whereas recent experiments show that remanent vortices can affect the low-temperature response of mechanical resonators even at low velocities.⁵⁰ At low velocities the drag in the normal liquid is dominated by viscosity.

The resulting fluid drag coefficient C_d^f is plotted in Fig. 4 as a function of the velocity amplitude. Measurements are shown for both the normal liquid at 4.2 K and for the superfluid at the lowest temperatures. The superfluid data show quite a sharp onset for turbulent drag at ~ 3 mm s⁻¹. At the highest velocities the drag coefficients for quantum (superfluid) and classical (normal liquid) turbulence are seen to be quite similar.

B. The inertial coefficient

The nondissipative fluid force F_m acting on the grid arises from the fluid backflow and can be considered as an enhancement of the effective mass of the grid. This is described in terms of an inertial coefficient C_m .⁴⁸ If we use the approximation that all parts of the grid are moving with the same velocity v , then we can define C_m by⁵¹

$$F_m = C_m \rho V \frac{dv}{dt}, \quad (5)$$

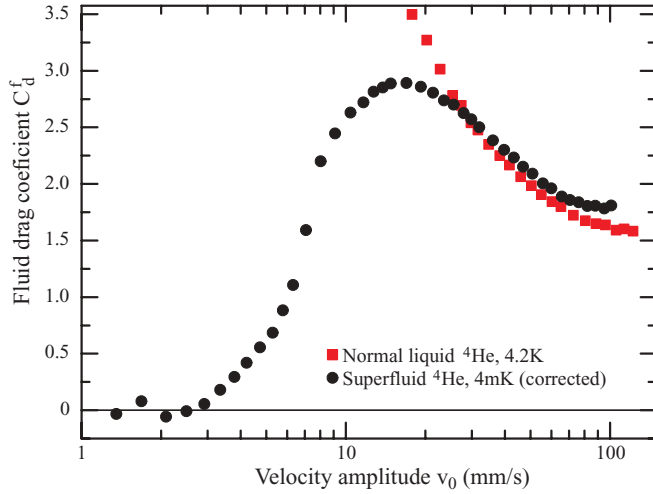


FIG. 4. (Color online) The drag coefficient of the vibrating grid, at its resonant frequency, as a function of its velocity amplitude, after subtracting the drag force measured in vacuum at $T \sim 4$ K. Red squares show measurements taken in normal liquid ^4He at $T = 4.2$ K. Circles show measurements taken at the lowest temperatures, ~ 4 mK after subtracting a slightly higher vacuum damping to leave only the contribution from the turbulent drag (see text).

where V is the solid volume of the grid. So C_m represents the effective mass of the fluid backflow expressed as a multiple of the mass of the fluid displaced by the stationary object. For a mechanical resonator, this leads to a shift in the resonant frequency given by⁵¹

$$\frac{\delta f}{f} = -\frac{1}{2} \frac{\rho}{\rho_w} C_m, \quad (6)$$

where ρ_w is the effective density of the material used to make the grid. As described in Sec. II, the grid mesh is made of copper, and the wire frame is copper-clad NbTi wire with a thin layer of insulation. The device also includes a small amount of glue. Thus it is difficult to determine a precise value for the effective density. In the following we assume a value equal to the density of copper $\rho = 8.94 \text{ g cm}^{-3}$ and we estimate the uncertainty to be $\sim 10\%$.

The frequency of the grid increases with increasing velocity as the grid enters the turbulent regime. This corresponds to a reduction in the inertial coefficient, shown in Fig. 5 for both superfluid and normal liquid helium. The inertial coefficient behaves quite differently for classical and quantum turbulence. For QT (the superfluid data), its magnitude rises sharply at a critical velocity of around $v_c \approx 3 \text{ mm s}^{-1}$, which coincides almost exactly with the observed critical velocity for the increase in the turbulent drag coefficient shown in Fig. 4. For classical turbulence (the normal liquid data), the inertial coefficient shows a small increase at a velocity close to the critical velocity v_c for QT. This is then followed by a faster increase at a velocity of $\sim 10 \text{ mm s}^{-1}$.

Unfortunately it is difficult to infer the inertial coefficient at higher velocities owing to the appearance of small background voltages (a small background voltage out of phase with the drive current mimics a frequency shift in the measurements since the resonant frequency is found by minimizing the out-

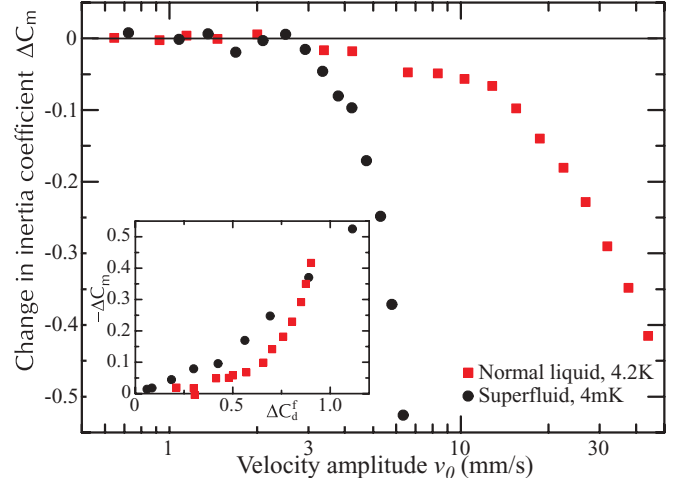


FIG. 5. (Color online) The change in the inertial coefficient of the vibrating grid, at its resonant frequency, as a function of its velocity amplitude. Squares show measurements taken in normal liquid ^4He at $T = 4.2$ K. Circles show measurements in superfluid ^4He at the lowest temperatures. Inset shows the corresponding reduction in the inertial coefficient as a function of the turbulent drag coefficient.

of-phase voltage). Over the limited velocity range shown in Fig. 5, the change in inertial coefficient has the same order of magnitude as the increase in the drag coefficient due to turbulence. This is shown in the inset to Fig. 5, where we plot the reduction in the inertial coefficient as a function of the turbulent drag coefficient. For the normal liquid data, in order to extract a “turbulent drag coefficient” we have subtracted a force linear in velocity from the total fluid force, to coincide with the measured laminar force at low velocities, i.e., we define the turbulent drag coefficient as the increase in the drag coefficient due to turbulence. We have done this for illustrative purposes only since, in reality, the forces from laminar and turbulent drag in a classical fluid are not additive. However, the inset illustrates that, as a function of the dissipative drag, normal fluid turbulence gives a sharper rise in the inertial coefficient compared to quantum turbulence.

V. POSITION MEASUREMENTS

The motion of the grid at arbitrary frequencies can be inferred from measurements of its position. This is done using the pick-up coils shown in Fig. 1. An alternating “probe” current is passed through the wire frame of the grid, superimposed on the drive current. The probe current induces voltage signals in the nearby pickup coils due to the mutual inductance.

The drive and probe currents are generated by a custom-made current source, which generates a current proportional to a linear supposition of two input voltages: a low-frequency “drive” input and a high-frequency “probe” input. The current passes through a high power standard resistor in series with the grid device. The probe current is controlled by a function generator which references three lock-in amplifiers; two to measure the voltages induced in the two pick-up coils and the third measures the voltage across the standard resistor to determine the amplitude of the probe current. The frequency

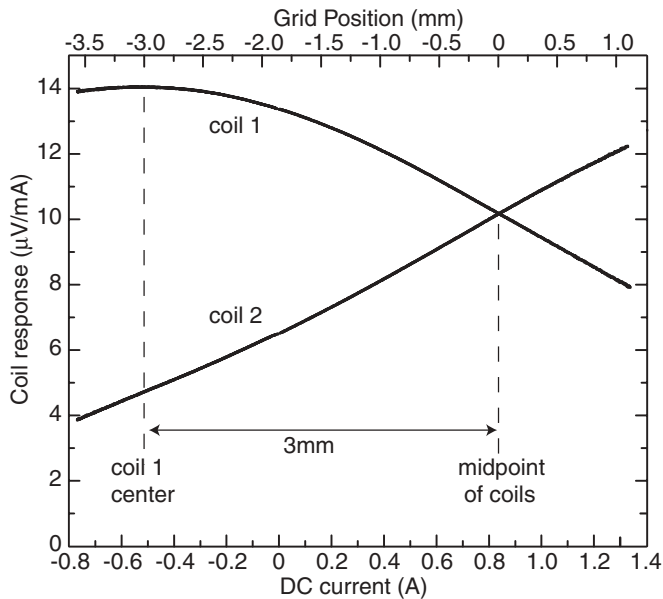


FIG. 6. The response (the induced voltage divided by the probe current) of the two pick-up coils as a function of the DC current applied to the grid device. The measurements are used to calibrate the position of the grid, by observing the features associated with (i) the grid being directly below the midpoint between the coils and (ii) the grid being directly below the center of the coil 1, as indicated. The inferred position of the grid relative to the midpoint between the coils is shown by the upper horizontal axis, see text.

of the probe current was fixed at ~ 90 kHz. Since this is very much higher than the resonant frequency of the device, the probe current does not produce any significant motion of the grid.

The voltage signals from the two coils depend on the relative position of the grid.⁴⁴ The coil signals can be calibrated to find the position of the grid as follows. The grid is deflected by passing a steady drive current through the wire frame. This is conveniently controlled by the voltage output of a data acquisition card. The drive current exerts a force F on the crossbar which generates a deflection described by

$$F = BDI = k\Delta x, \quad (7)$$

where Δx is the horizontal displacement of the crossbar of the grid relative to its equilibrium position and k is the effective spring constant.

Figure 6 shows the response (the induced voltage divided by the probe current) of the two pickup coils as a function of the steady current applied to the grid. The response from each pickup coil passes through a maximum as the crossbar of the device passes below its center. Since the two coils are a known distance apart (6 mm), we can determine the absolute position of the crossbar.

In practice, the device shows hysteretic behavior which becomes most apparent above a critical current of $\sim I = 1.5$ A. When higher currents are applied the response changes discontinuously, accompanied by a change in the equilibrium position with zero current (we have observed changes of order 1 mm). The equilibrium position with zero current can also be changed by changing the vertical magnetic field. We presume

that this behavior is due to trapped flux lines in the NbTi filament in wire frame of the device; the trapped flux is able to exert sufficient force to deflect the grid significantly and to change the restoring force. Flux pinning results in hysteretic behavior, dependent on both the magnetic field and the applied current. To minimize these effects for the measurements presented here, the current was always kept well below the critical current. In this case the hysteresis on changing the current was found to be very small, typically $< 1\%$. (We further note that the hysteresis may be significantly reduced by using multifilamentary superconducting wire for the wire frame, instead of the single filament wire used for the device discussed here.)

Consider the data shown in Fig. 6, starting from a steady current of $I \sim -0.8$ A. The device is initially deflected beyond coil 1. As the current is ramped upwards, the device moves closer to the coils and the coil responses increase. As the device moves below the center of coil 1 the response of coil 1 passes through a maximum. As the current reaches $I \sim +0.8$ A, the two coil responses become equal as the device moves to the midpoint between the two coils. On further increasing the current, the coil 2 response continues to increase and the coil 1 response continues to decrease as the device approaches coil 2. If the current is increased sufficiently, the coil 2 response will also pass through a maximum as the grid moves below its center. However, the response is found to change discontinuously at ~ 1.5 A due to a redistribution of the trapped flux lines as discussed above.

From the data shown in Fig. 6, we can identify the values of the steady current I_1 and I_m at which the crossbar of the device passes below the center of coil 1 and the midpoint between the coils, respectively. From this, the spring constant can be found using Eq. (7), giving $k = \Delta I_0 BD / \Delta X_0$, where $\Delta I_0 = I_1 - I_m$ and $\Delta X_0 = 3$ mm is the distance between the center of coil 1 and the midpoint between the coils. The position of the crossbar, relative to the midpoint between the two coils, as a function of the steady current I , can then be found using

$$x = \Delta X_0 \frac{I - I_m}{\Delta I_0}. \quad (8)$$

The inferred position is shown by the upper horizontal axis in Fig. 6. The data in Fig. 6 can now be used to infer the position of the grid from the coil response, independently of the applied current. For dynamic measurements, the velocity of the grid is simply found from the time derivative of the position. Below, we describe measurements in which we use this technique to study the response of superfluid ^4He to the grid motion over a broad range of frequencies.

VI. OFF-RESONANT RESPONSE

To oscillate the device at an arbitrary angular frequency ω , a drive current $I_0 \exp(i\omega t)$ is supplied by the custom current supply which is controlled by a function generator, the “drive current generator.” The equilibrium position of the grid is adjusted, using a superimposed steady current, to move the grid into a position where at least one of the coils produces a roughly linear response with changing position. In practice an equilibrium position close to the midpoint between the two

coils is chosen for this purpose, giving a region which is linear to within a few percent over a range of 1 mm or more in displacement.

For the measurements described here, the damping forces are not very large compared to the restoring and/or inertial forces on the oscillating grid. In this case, the grid oscillates sinusoidally to a good approximation. So in a region where a given coil voltage varies linearly with position, the oscillation induces a sinusoidal modulation of the coil signal. This is measured by an additional lock-in amplifier. The analog output of the lock-in used to measure the coil signal is fed into the input of a second lock-in amplifier which is referenced to the drive current generator. This second lock-in then measures the amplitude and phase of the oscillating coil signal which gives a direct measure of the amplitude and phase of the oscillating grid position using the calibration procedure described in Sec. V. Particular care is taken to characterize and account for the finite measurement time constant of the first lock-in amplifier because this introduces a small additional phase shift. From these measurements we can infer the oscillating position of the grid as

$$x = x_0 \exp(i\omega t) \exp(i\theta), \quad (9)$$

where x_0 is the amplitude of the oscillation and θ is the phase shift with respect to the drive current $I_0 \exp(i\omega t)$, obtained from the measured coil signal oscillation after correcting for the finite time constant of the first lock-in amplifier.

For a given drive current amplitude I_0 , the displacement amplitude tends to a constant value, $x_0 = BDI_0/k$, at low frequencies and the phase shift tends to zero. The amplitude passes through a maximum on resonance with $\theta = 90^\circ$. At higher frequencies, the amplitude falls and the phase shift tends towards $\theta = 180^\circ$.

To infer the dissipative drag force exerted on the grid, we consider the power dissipated. Assuming a sinusoidal response, the average power dissipated is

$$\dot{Q} = \frac{1}{2} F_0 v_0 \sin \theta, \quad (10)$$

where $F_0 = BDI_0$ is the amplitude of the driving force and $v_0 = \omega x_0$ is the resulting velocity amplitude of the oscillation. The dissipation arises from the dissipative drag force F_d , which is always in phase with the velocity of the grid. The average power dissipated can thus be written as $\dot{Q} = \frac{1}{2} F_d^0 v_0$, where F_d^0 is the amplitude of the dissipative drag force. For the measurements described here, the situation is more complicated since the velocity of the grid is not spatially uniform and in general the drag force varies nonlinearly with velocity. In this case F_d^0 should be considered as an appropriately time- and spatially averaged amplitude of the dissipative drag force. We note that the drag forces inferred from resonant velocity measurements, such as those shown in Fig. 2, represent the same appropriately time- and spatially averaged amplitudes. The amplitude of the drag force is thus given by

$$F_d^0 = F_0 \sin \theta. \quad (11)$$

In Fig. 7 we plot the velocity amplitude of the grid motion as a function of the amplitude of the (averaged) drag force inferred from Eq. (11). The data are compared directly with the resonant velocity measurements from Fig. 2. The position

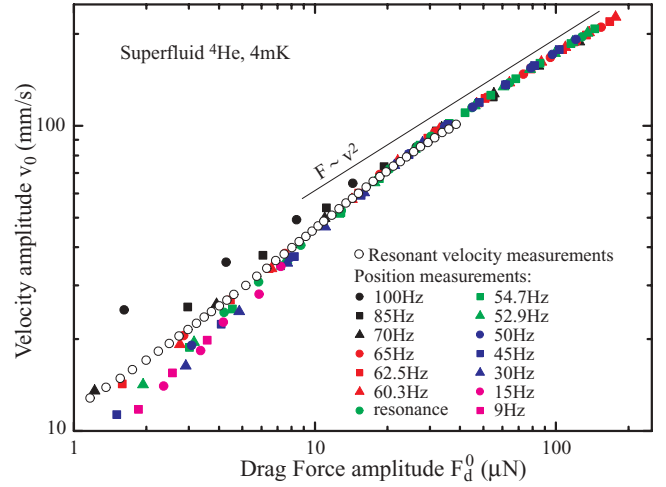


FIG. 7. (Color online) The velocity amplitude of the grid as a function of the dissipative drag force in superfluid ^4He at very low temperatures. Open circles show the data measured at the resonance frequency using the velocity measurement technique (this is the same data shown in Fig. 2). Filled symbols correspond to data taken using the position measurement technique, at various frequencies.

measurements extend up to higher velocities, since these do not suffer problems with the background voltages that limit the resonant velocity measurements. The drag force remains roughly proportional to the square of the velocity, indicating that the drag coefficient remains roughly constant up to 200 mm s^{-1} . For the position measurements, we limit the amplitude of the displacement to around $x_0^{\text{max}} \approx 0.5 \text{ mm}$ to ensure that the coil response always varies linearly with velocity.

The data in Fig. 7 show a reasonably good agreement between the response inferred from the resonant velocity measurements and that inferred from the position measurements. The very striking result revealed in Fig. 7 is that the response of the grid in the turbulent regime, particularly at higher velocities, is independent of frequency over the measurement range from 9 to 100 Hz.

It is difficult to extend the measurements to much higher or much lower frequencies, because the phase shift θ becomes very close to 0 or 180° . In this case small errors in the phase measurement (e.g., from the finite time constant of the first lock-in amplifier) generate large errors in the inferred drag force. This problem becomes particularly apparent for small drag forces, so the apparent deviations of the data at low velocities in Fig. 7 probably result from small errors in the phase measurement.

VII. DISCUSSION

We compare our results with measurements on other vibrating objects in superfluid ^4He and in classical fluids. First, consider the measurements of the fluid drag coefficient in normal liquid ^4He shown in Fig. 4. At low velocities the drag is dominated by viscous dissipation, while at higher velocities the fluid drag coefficient tends towards a constant, $C_d^f \approx 1.6$, which we associate with turbulent drag. Similar values are found for the turbulent drag experienced by cylinders in classical fluids.^{52,53} Oscillating grids have been

studied in classical fluids⁵⁴ but we are not aware of any other measurements of the turbulent drag coefficients for grids oscillating in classical fluids. For uniformly moving grids typical values of the drag coefficient at high velocities vary from around 2.1 to 4.5 depending on the precise geometry and other conditions: smaller values are usually measured for smooth grids, and higher values are measured for grids with sharp corners and/or at very high Reynolds numbers.⁵⁵

The drag coefficients for QT in superfluid ⁴He at high velocities display a broad range of values for different objects. Many measurements on vibrating spheres and vibrating wires give values for the turbulent drag coefficient in the range of $C_d \approx 0.1$ to $C_d \approx 0.4$.^{29,56} Tuning forks also show a broad variation from $C_d \approx 0.2$ to $C_d \approx 1$ even for forks with similar dimensions and resonant frequencies.^{29,56} Previous measurements on a grid vibrating at ~ 1 kHz gave $C_d \approx 0.1$ at the highest measured velocities,^{33,56} but the velocities were too small to identify a limiting value.

Comparing the drag coefficients at high velocities for QT and classical turbulence (the normal liquid and superfluid data, respectively, in Fig. 4), we see that they have very similar values. This demonstrates the strong similarities between QT and classical turbulence: even though the two forms of turbulence must behave very differently on length scales smaller than the vortex line spacing in QT, they produce very similar drag forces at high velocities. A similar result was previously reported for tuning fork resonators.²⁹

A reduction in the inertial coefficient due to turbulent flow has been observed for oscillatory flows of classical fluids past cylinders,^{52,53} and has also been observed for vibrating wire resonators in superfluid ⁴He.^{25,51} Referring to Fig. 5, the reduction in the inertial coefficient occurs more suddenly at the onset of QT compared to classical turbulence. This difference is also apparent when the changes in the inertial coefficient are plotted against the turbulent drag coefficient shown in the inset to Fig. 5. At low turbulent drag coefficients, the inertial coefficient shows a greater reduction for QT compared to classical turbulence. We also note that for QT the reduction in the inertial coefficient varies linearly with the turbulent drag coefficient at low velocities, and a similar result was previously reported for vibrating wire resonators in superfluid ⁴He.⁵¹

Next, we discuss the critical velocities for QT. In superfluid ⁴He, there is growing evidence⁵⁷ that critical velocities for the onset of turbulent drag for vibrating objects are frequency dependent, given approximately by

$$v_c \sim \sqrt{8\kappa\omega}. \quad (12)$$

For our grid this expression predicts a critical velocity of $v_c \sim 17$ mm/s, which is considerably higher than our measured value of 3 mm/s. At first sight, this is a puzzling result. One might anticipate that the critical velocity should become independent of frequency at sufficiently low frequencies, where the flow essentially mimics uniform flow, but this would result in a critical velocity *higher* than the value predicted by Eq. (12). However, as noted in Ref. 58, there is likely to be a geometry dependence of the critical velocity since an important parameter is the maximum relative velocity between the superfluid and the surface of the object. The grid mesh used in our measurements has a large aspect ratio perpendicular to

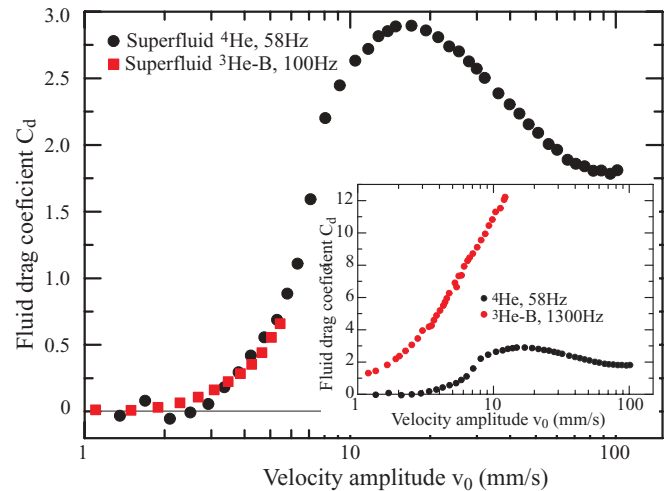


FIG. 8. (Color online) A comparison of the turbulent drag coefficient as a function of velocity for similar low-frequency vibrating grids in superfluid ⁴He (black circles) and superfluid ³He-B (red squares). Inset shows a comparison of the low-frequency grid in superfluid ⁴He (black circles) with a grid vibrating at a much higher frequency in superfluid ³He-B. All of the data were taken in the zero-temperature limit.

its motion: the copper strips which form the mesh are ≈ 11 μm wide but only ≈ 1 μm thick. Subsequently there will be a large enhancement of the local superfluid flow around the edges of the grid mesh which will reduce the measured critical velocity.

VIII. COMPARISON WITH ³He-B

We compare our measurements with those of similar vibrating grids, which use the *same* grid mesh material, in superfluid ³He-B at low temperatures. It is particularly interesting to compare turbulent behavior in different superfluids. The circulation quantum in ³He-B is $\sim 30\%$ smaller and the vortex core size is more than 100 times larger than that in superfluid ⁴He.

In Fig. 8 we compare our measurements of the dissipative turbulent drag coefficient in superfluid ⁴He at low temperatures with measurements made on a similar low-frequency grid in superfluid ³He-B. The grid used for the ³He-B measurements was somewhat smaller, of dimensions 5.6×5 mm, supported by a frame of 50 μm CuNi-clad NbTi multifilamentary wire with a leg spacing of 5 mm and a height of 12 mm. The measurements in superfluid ³He-B were taken at temperatures between 150 and 320 μK at 3.8 bar pressure. To obtain the turbulent drag force we have subtracted the thermal drag force^{59–61} in a manner similar to that described in Ref. 62 and we have also subtracted a linear intrinsic drag force.

The data in Fig. 8 show that, at low frequencies, the turbulent drag in the two superfluids is virtually identical. So the turbulent drag is insensitive to the circulation quantum and the vortex core size. It would be interesting to extend the measurements in superfluid ³He-B to higher velocities, but this is quite difficult since the dissipation at ultralow temperatures causes the cell to warm significantly.

The inset in Fig. 8 shows the comparison with another grid in ³He-B. This grid used the same mesh material,

but it had a thicker wire frame resulting in a much higher resonant frequency of ~ 1300 Hz. The turbulent drag for this grid is clearly much larger reaching values of order 10 at a velocity of 10 mm s^{-1} . Similarly high drag coefficients were previously reported for other vibrating grids in $^3\text{He-B}$ with different grid meshes and with resonant frequencies of order 1 kHz.^{13,62} Various experiments with these grids in $^3\text{He-B}$ show that vortex rings are emitted at low grid velocities^{8,63,64} which subsequently develop into QT for grid velocities above $\sim 3 \text{ mm s}^{-1}$.^{9,13,64,65}

To address the large drag at higher frequencies, we first consider the behavior of other vibrating objects in $^3\text{He-B}$. Here, the response of vibrating wires and tuning forks is dominated by pair breaking at high velocities. The Landau critical velocity corresponds to the minimum in the quasiparticle excitation curve giving $v_L \approx \Delta/p_F \approx 30 \text{ mm s}^{-1}$, where Δ is the energy gap and p_F is the Fermi momentum. The critical velocity for vibrating wire resonators^{66,67} and tuning forks⁵⁶ is found to occur at a fraction (typically one-third) of the Landau critical velocity due to the presence of bound quasiparticle states at the surface of the oscillator; pair breaking can occur below the Landau velocity provided that at least one of the two excitations generated occupies a bound state which has an energy below the bulk energy gap.^{68,69} For vibrating wires, vortex lines are also generated above this critical velocity.^{70,71} However, we note that recent measurements with low-frequency vibrating wires show that vortices can also be created at a critical velocity consistent with Eq. (12) provided that this is lower than the pair-breaking critical velocity.⁷²

The pair-breaking mechanism^{68,69} in $^3\text{He-B}$ depends on the frequency. At very low frequencies, the bound states become filled, so pair breaking only occurs transiently (for uniform motion the critical velocity must be the full Landau critical velocity). So we may speculate that for the low-frequency grid, pair breaking plays no role and the drag coefficient is due to the growth of remanent vortices which eventually leads to turbulence via the same mechanisms responsible in superfluid ^4He . This would explain the near identical drag coefficients for the low-frequency grids shown in Fig. 8. The higher drag coefficients observed at higher frequencies in $^3\text{He-B}$, shown in the inset to Fig. 8, suggest that pair breaking could be playing a significant role in this case. The critical velocity for pair breaking for these grids could be very small since the grid mesh is very flat with sharp corners (see Fig. 1) which will greatly enhance the local backflow. We further speculate that in this case pair breaking may assist the growth of vortex lines

and/or facilitate intrinsic nucleation of vortices, which will produce extra drag.

We note that intrinsic nucleation was previously suggested as an explanation for the larger drag in $^3\text{He-B}$,⁷³ and we further note that the critical velocity for intrinsic vortex nucleation is quite similar to the critical velocity for pair breaking.^{73,74} In contrast, intrinsic nucleation should not play any role in superfluid ^4He since the critical velocity is orders of magnitude higher. The role of intrinsic and extrinsic mechanisms is an interesting topic for future research.

IX. SUMMARY

We have presented measurements of both the inertial and dissipative drag coefficients for a low-frequency vibrating grid in liquid ^4He . Measurements in normal and superfluid helium at very low temperatures allow us to compare the behavior of the drag coefficients for classical and pure quantum turbulence. The dissipative turbulent drag is quite similar at high velocities, but the inertial drag coefficient shows a much sharper onset for quantum turbulence. We have introduced a measurement technique to investigate the dissipative drag coefficient down to very low frequencies. We find that the turbulent drag is independent of frequency, which suggests that we can use these devices to study turbulence generated from quasistatic motion through superfluids at very low temperatures. We have also shown that the turbulent drag on grids at low frequencies and velocities is virtually identical for superfluid ^4He and superfluid $^3\text{He-B}$, which implies that the drag is insensitive to the quantum of circulation and the vortex core size. Further measurements on different devices are needed to determine whether this is a general feature of quantum turbulence. At higher frequencies, the drag on grids in superfluid $^3\text{He-B}$ is significantly enhanced. We believe that this is due to pair breaking, but the precise mechanisms remain unknown.

ACKNOWLEDGMENTS

We thank S. M. Holt for the design and construction of the current supply for the grid device. We acknowledge M. G. Ward and A. Stokes for excellent technical support, and useful discussions with A. I. Golov, W. Guo, G. G. Ihas, D. N. McKinsey, P. Skyba, K. J. Thompson, W. F. Vinen, and P. M. Walmsley. The work was supported by the UK EPSRC MWN programme, the Leverhulme Trust, and by the EU-funded Integrating Activity project MICROKELVIN, Grant No. 228464.

*s.fisher@lancaster.ac.uk

¹W. F. Vinen and J. J. Niemela, *J. Low Temp. Phys.* **128**, 167 (2002).

²S. W. V. Sciver and C. F. Barenghi, *Prog. Low Temp. Phys.* **16**, 247 (2009).

³L. Skrbek and K. R. Sreenivasan, *Phys. Fluids* **24**, 011301 (2012).

⁴S. Fujiyama, A. Mitani, M. Tsubota, D. I. Bradley, S. N. Fisher, A. M. Guénault, R. P. Haley, G. R. Pickett, and V. Tsepelin, *Phys. Rev. B* **81**, 180512 (2010).

⁵K. W. Schwarz, *Phys. Rev. B* **31**, 5782 (1985).

⁶M. Tsubota, T. Araki, and S. K. Nemirovskii, *Phys. Rev. B* **62**, 11751 (2000).

⁷D. I. Bradley, S. N. Fisher, A. M. Guénault, M. R. Lowe, G. R. Pickett, A. Rahm, and R. C. V. Whitehead, *Phys. Rev. Lett.* **93**, 235302 (2004).

⁸D. I. Bradley, D. O. Clubb, S. N. Fisher, A. M. Guénault, R. P. Haley, C. J. Matthews, G. R. Pickett, V. Tsepelin, and K. Zaki, *Phys. Rev. Lett.* **95**, 035302 (2005).

- ⁹D. I. Bradley, D. O. Clubb, S. N. Fisher, A. M. Guénault, R. P. Haley, C. J. Matthews, G. R. Pickett, V. Tsepelin, and K. Zaki, *Phys. Rev. Lett.* **96**, 035301 (2006).
- ¹⁰P. M. Walmsley, A. I. Golov, H. E. Hall, A. A. Levchenko, and W. F. Vinen, *Phys. Rev. Lett.* **99**, 265302 (2007).
- ¹¹P. M. Walmsley and A. I. Golov, *Phys. Rev. Lett.* **100**, 245301 (2008).
- ¹²D. I. Bradley, S. N. Fisher, A. M. Guénault, R. P. Haley, S. O'Sullivan, G. R. Pickett, and V. Tsepelin, *Phys. Rev. Lett.* **101**, 065302 (2008).
- ¹³D. I. Bradley, S. N. Fisher, A. M. Guénault, R. P. Haley, G. R. Pickett, D. Potts, and V. Tsepelin, *Nat. Phys.* **7**, 473 (2011).
- ¹⁴J. D. Reppy and D. Depatie, *Phys. Rev. Lett.* **12**, 187 (1964).
- ¹⁵P. L. Gammel, H. E. Hall, and J. D. Reppy, *Phys. Rev. Lett.* **52**, 121 (1984).
- ¹⁶L. Landau, *J. Phys. (USSR)* **5**, 71 (1941).
- ¹⁷L. Landau, *J. Phys. (USSR)* **11**, 91 (1947).
- ¹⁸T. Ellis and P. V. E. McClintock, *Philos. Trans. R. Soc. London, Ser. A* **315**, 259 (1985).
- ¹⁹D. D. Awschalom and K. W. Schwarz, *Phys. Rev. Lett.* **52**, 49 (1984).
- ²⁰L. Skrbek and W. Vinen, *Prog. Low Temp. Phys.* **16**, 195 (2009).
- ²¹R. Goto, S. Fujiyama, H. Yano, Y. Nago, N. Hashimoto, K. Obara, O. Ishikawa, M. Tsubota, and T. Hata, *Phys. Rev. Lett.* **100**, 045301 (2008).
- ²²A. C. H. Hallett, *Prog. Low Temp. Phys.* **1**, 64 (1955).
- ²³R. J. Donnelly and O. Penrose, *Phys. Rev.* **103**, 1137 (1956).
- ²⁴R. J. Donnelly and A. C. H. Hallett, *Ann. Phys.* **3**, 320 (1958).
- ²⁵D. I. Bradley, D. O. Clubb, S. N. Fisher, A. M. Guénault, R. P. Haley, C. J. Matthews, G. R. Pickett, and K. L. Zaki, *J. Low Temp. Phys.* **138**, 493 (2005).
- ²⁶H. Yano, Y. Nago, R. Goto, K. Obara, O. Ishikawa, and T. Hata, *Phys. Rev. B* **81**, 220507 (2010).
- ²⁷D. I. Bradley, A. M. Guénault, S. N. Fisher, R. P. Haley, M. J. Jackson, D. Nye, K. O'Shea, G. R. Pickett, and V. Tsepelin, *J. Low Temp. Phys.* **162**, 375 (2011).
- ²⁸R. Blaauwgeers, M. Blazkova, M. Clovecko, V. B. Eltsov, R. de Graaf, J. Hosio, M. Krusius, D. Schmoranzner, W. Schoepe, L. Skrbek *et al.*, *J. Low Temp. Phys.* **146**, 537 (2007).
- ²⁹M. Blazkova, D. Schmoranzner, L. Skrbek, and W. F. Vinen, *Phys. Rev. B* **79**, 054522 (2009).
- ³⁰D. I. Bradley, M. J. Fear, S. N. Fisher, A. M. Guénault, R. P. Haley, C. R. Lawson, P. V. E. McClintock, G. R. Pickett, R. Schanen, V. Tsepelin *et al.*, *J. Low Temp. Phys.* **156**, 116 (2009).
- ³¹W. Schoepe, *Phys. Rev. Lett.* **92**, 095301 (2004).
- ³²S. I. Davis, P. C. Hendry, and P. V. E. McClintock, *Physica B* **280**, 43 (2000).
- ³³D. Charalambous, L. Skrbek, P. C. Hendry, P. V. E. McClintock, and W. F. Vinen, *Phys. Rev. E* **74**, 036307 (2006).
- ³⁴J. C. Bennett and S. Corrsin, *Phys. Fluids* **21**, 2129 (1978).
- ³⁵A. L. Kistler and T. Vrebalovich, *J. Fluid Mech.* **26**, 37 (1966).
- ³⁶M. Tsubota and M. Kobayashi, *Prog. Low Temp. Phys.* **16**, 1 (2009).
- ³⁷S. R. Stalp, L. Skrbek, and R. J. Donnelly, *Phys. Rev. Lett.* **82**, 4831 (1999).
- ³⁸L. Skrbek, J. J. Niemela, and R. J. Donnelly, *Phys. Rev. Lett.* **85**, 2973 (2000).
- ³⁹G. G. Ihas, G. Labbe, S. C. Liu, and K. J. Thompson, *J. Low Temp. Phys.* **150**, 384 (2008).
- ⁴⁰S. M. Thompson and J. S. Turner, *J. Fluid Mech.* **67**, 349 (1975).
- ⁴¹E. J. Hopfinger and J. A. Toly, *J. Fluid Mech.* **78**, 155 (1976).
- ⁴²R. R. Long, *Phys. Fluids* **21**, 1887 (1978).
- ⁴³S. Fisher and G. Pickett, *Prog. Low Temp. Phys.* **16**, 147 (2009).
- ⁴⁴D. I. Bradley, M. Človečko, M. J. Fear, S. N. Fisher, A. M. Guénault, R. P. Haley, C. R. Lawson, G. R. Pickett, R. Schanen, V. Tsepelin *et al.*, *J. Low Temp. Phys.* **165**, 114 (2011).
- ⁴⁵D. I. Bradley, T. W. Bradshaw, A. M. Guénault, V. Keith, B. G. Locke-Scobie, I. E. Miller, G. R. Pickett, and W. P. Pratt, *Cryogenics* **22**, 296 (1982).
- ⁴⁶D. C. Carless, H. E. Hall, and J. R. Hook, *J. Low Temp. Phys.* **50**, 583 (1983).
- ⁴⁷G. G. Stokes, *Trans. Cambridge Philos. Soc.* **9**, 8 (1852).
- ⁴⁸J. R. Morison, M. P. O'Brien, J. W. Johnson, and S. A. Schaaf, *Petroleum Transactions* **189**, 149 (1950).
- ⁴⁹D. I. Bradley, M. Človečko, S. N. Fisher, D. Garg, E. Guise, R. P. Haley, O. Kolosov, G. R. Pickett, V. Tsepelin, D. Schmoranzner *et al.*, *Phys. Rev. B* **85**, 014501 (2012).
- ⁵⁰N. Hashimoto, R. Goto, H. Yano, K. Obara, O. Ishikawa, and T. Hata, *Phys. Rev. B* **76**, 020504 (2007).
- ⁵¹D. I. Bradley, S. N. Fisher, A. M. Guénault, R. P. Haley, V. Tsepelin, G. R. Pickett, and K. L. Zaki, *J. Low Temp. Phys.* **154**, 97 (2009).
- ⁵²T. Sarpkaya, *J. Fluid Mech.* **165**, 62 (1986).
- ⁵³E. D. Obasaju, P. W. Bearman, and J. M. R. Graham, *J. Fluid Mech.* **196**, 467 (1988).
- ⁵⁴I. P. D. de Silva and H. J. S. Fernando, *Phys. Fluids* **6**, 2455 (1994).
- ⁵⁵R. C. Higginson, S. B. Dalziel, and P. F. Linden, *Exp. Fluids* **34**, 678 (2003).
- ⁵⁶D. I. Bradley, P. Crookston, S. N. Fisher, A. Ganshin, A. M. Guénault, R. P. Haley, M. J. Jackson, G. R. Pickett, R. Schanen, and V. Tsepelin, *J. Low Temp. Phys.* **157**, 476 (2009).
- ⁵⁷R. Hänninen and W. Schoepe, *J. Low Temp. Phys.* **153**, 189 (2008).
- ⁵⁸R. Hänninen and W. Schoepe, *J. Low Temp. Phys.* **164**, 1 (2011).
- ⁵⁹S. N. Fisher, A. M. Guénault, C. J. Kennedy, and G. R. Pickett, *Phys. Rev. Lett.* **63**, 2566 (1989).
- ⁶⁰S. N. Fisher, G. R. Pickett, and R. J. Watts-Tobin, *J. Low Temp. Phys.* **83**, 225 (1991).
- ⁶¹M. P. Enrico, S. N. Fisher, and R. J. Watts-Tobin, *J. Low Temp. Phys.* **98**, 81 (1995).
- ⁶²D. I. Bradley, D. O. Clubb, S. N. Fisher, A. M. Guénault, C. J. Matthews, and G. R. Pickett, *J. Low Temp. Phys.* **134**, 381 (2004).
- ⁶³D. I. Bradley, S. N. Fisher, A. M. Guénault, R. P. Haley, C. J. Matthews, G. R. Pickett, J. Roberts, S. O'Sullivan, and V. Tsepelin, *J. Low Temp. Phys.* **148**, 235 (2007).
- ⁶⁴D. I. Bradley, S. N. Fisher, A. M. Guénault, R. P. Haley, M. Holmes, S. O'Sullivan, G. R. Pickett, and V. Tsepelin, *J. Low Temp. Phys.* **150**, 364 (2008).
- ⁶⁵D. I. Bradley, S. N. Fisher, A. M. Guénault, R. P. Haley, C. J. Matthews, G. R. Pickett, V. Tsepelin, and K. Zaki, *Low Temperature Physics, Pts. A and B*, AIP Conf. Proc. No. 850 (AIP, Melville, NY, 2006), p. 173.
- ⁶⁶S. N. Fisher, A. M. Guénault, C. J. Kennedy, and G. R. Pickett, *Phys. Rev. Lett.* **69**, 1073 (1992).
- ⁶⁷S. N. Fisher, A. M. Guénault, C. J. Kennedy, and G. R. Pickett, *Phys. Rev. Lett.* **67**, 1270 (1991).

- ⁶⁸C. J. Lambert, *Physica B* **178**, 294 (1992).
- ⁶⁹A. Calogeracos and G. E. Volovik, *JETP* **88**, 40 (1999).
- ⁷⁰S. N. Fisher, A. J. Hale, A. M. Guénault, and G. R. Pickett, *Phys. Rev. Lett.* **86**, 244 (2001).
- ⁷¹D. I. Bradley, S. N. Fisher, A. M. Guénault, M. R. Lowe, G. R. Pickett, and A. Rahm, *Physica B* **329–333**, 104 (2003).
- ⁷²Y. Nago, M. Inui, R. Kado, K. Obara, H. Yano, O. Ishikawa, and T. Hata, *Phys. Rev. B* **82**, 224511 (2010).
- ⁷³R. Hänninen, M. Tsubota, and W. F. Vinen, *Phys. Rev. B* **75**, 064502 (2007).
- ⁷⁴V. M. H. Ruutu, Ü. Parts, J. H. Koivuniemi, N. B. Kopnin, and M. Krusius, *J. Low Temp. Phys.* **107**, 93 (1997).